

Low loss liquid crystals for infrared applications

Fenglin Peng^a, Yuan Chen^a, Shin-Tson Wu^{a*}, Suvagata Tripathi^b and Robert J. Twieg^b

^aCREOL, The College of Optics and Photonics, University of Central Florida, Orlando, FL, USA; ^bDepartment of Chemistry, Kent State University, Kent, OH, USA

(Received 16 May 2014; accepted 4 June 2014)

Seven fluorinated and chlorinated terphenyl compounds intended for mid-wave infrared (MWIR) applications are synthesised and two eutectic mixtures formulated, and their physical properties evaluated. In addition to low absorption, some desirable properties for MWIR applications include wide nematic range, high birefringence, large dielectric anisotropy and low viscosity. The fluorinated terphenyl mixture exhibits a relatively low absorption in the vicinities of $\lambda \sim 3 \mu\text{m}$, but a fairly strong overtone appears in the 4–5 μm region. To suppress these overtone absorptions, short-chain chlorinated terphenyl compounds are proven to be useful.

Keywords: liquid crystal; low absorption; mid-wave infrared

1. Introduction

In addition to displays (amplitude modulation), nematic liquid crystal (LC) is also a strong contender for phase modulation, such as spatial light modulators (SLMs), [1] laser beam steering, [2,3] adaptive optics, adaptive lenses, [4] and phase shifters in the microwave [5,6] and terahertz [7–9] regions. To achieve phase modulation, two types of device structures have been demonstrated: (1) deflective beam steering using an optical phased array (OPA), [2] and (2) refractive beam steering using a waveguide structure. [10,11] In a deflective OPA, 2π modulo is generally required. The phase change (δ) of a SLM is governed by following equation:

$$\delta = 2\pi d\Delta n/\lambda \quad (1)$$

where d is the cell gap, Δn is the LC birefringence and λ is the wavelength. From Equation (1), to obtain $\delta = 2\pi$ we need $d\Delta n = \lambda$. In the visible spectral region, say $\lambda = 0.5 \mu\text{m}$, this condition can be easily satisfied. But as the wavelength increases to mid-wave infrared (MWIR, say $\lambda = 5 \mu\text{m}$), the required $d\Delta n$ is $10\times$ larger. Moreover, as λ increases, Δn decreases and then saturates, according to the single-band birefringence dispersion model. [12,13] Let us use $\Delta n = 0.2$ as an example. The required LC layer thickness is $d = 25 \mu\text{m}$, which leads to a relatively slow response time (>100 ms). To overcome the slow response time problem, refractive beam steering with a waveguide LC structure has been demonstrated. In the waveguide approach, the optical path length is 3–5 mm, so that the accumulated phase change is large. As a result, the steering angle as large as 270° has been

demonstrated in the 1D device, and $50^\circ \times 15^\circ$ in the 2D beam steerer. The response time is also very fast because only the first few surface layers contribute to modulating the penetrated evanescent waves. Although the refractive device offers so many attractive properties, its biggest challenge is absorption loss. The transmittance of a scattering-free LC device is governed by:

$$T = \exp(-\alpha\ell) \quad (2)$$

where α stands for the absorption coefficient at a laser wavelength λ and ℓ is the optical path length. In the visible region, both α and ℓ are small so that the absorption loss can be completely neglected. But in the MWIR region, α can reach 10 cm^{-1} or higher. For a 3-mm waveguide, the absorption loss would be 95%. Fortunately, in the refractive beam steerer the LC serves as a cladding layer, and only about 10% of the evanescent beam penetrates into the LC layer. Therefore, the equivalent optical loss is about $10\times$ smaller than that if the beam was directly propagating in the LC medium, in which light scattering loss would be intolerable. After having taken this factor of 10 into consideration, the optical loss is still 25%. The absorbed light will turn into heat, which in turn affects the LC properties. Therefore, there is an urgent need to develop new nematic LC materials with high birefringence, large dielectric anisotropy and more importantly low absorption coefficient.

From absorption viewpoint, the $\pi \rightarrow \pi^*$ electronic transitions of a conjugated LC occur in the UV region. [14] As the molecular conjugation increases, the resonance wavelength increases gradually. In the

*Corresponding author. Email: swu@ucf.edu

visible to near infrared ($\sim 1 \mu\text{m}$) region, most LCs are quite transparent, except some coloured LC dyes. As the wavelength keeps increasing, molecular vibrations, e.g., CH stretching, CN stretching, C=C stretching in the phenyl rings, C–H in-plane deformation, C–C skeletal stretching, C–F stretching and C–H out-of-plane deformation, etc. take place in the MWIR (3–5 μm) and long-wave infrared (LWIR 8–12 μm) regions.[15] In MWIR, several notable molecular vibration bands exist, such as CH, CH₂, CH₃, CN, C≡C, and NCS stretching. The CH, CH₂ and CH₃ absorption bands overlap closely and form a strong absorption band covering from 3.2 to 3.7 μm .[16] These carbon-hydrate bonds in the alkyl chain or in the aromatic rings are basic elements for an organic compound to exhibit mesogenic phase. On the other hand, the narrow but strong cyano (CN) and tolane (C≡C) absorption peaks occur at $\sim 4.45 \mu\text{m}$ while isothiocyanato (NCS) polar group has a broad and strong absorption band in the 4.5–5.2 μm region. In addition to low absorption, following properties are equally important for MWIR applications: wide nematic temperature range, high birefringence (Δn), low viscosity and large dielectric anisotropy ($\Delta\epsilon$). Wide nematic range can be achieved by formulating eutectic mixtures. High birefringence is desired in order to achieve a certain phase change (2π for an OPA) with a minimum cell gap (d) since the response time of a LC device is proportional to d^2 .[17] Last but not the least, a large $\Delta\epsilon$ helps to reduce the operation voltage.

The molecular vibration frequency (ω) depends on the spring constant (κ) and reduced mass (μ) of the diatomic group as:

$$\omega = \sqrt{\kappa/\mu} \quad (3)$$

As the reduced mass increases the vibration frequency decreases, i.e., the absorption band shifts towards a longer wavelength. From Equation (3), three approaches can be considered for shifting the absorption bands outside the spectral region of interest: deuteration,[18–20] fluorination [21,22] and chlorination.[23,24]

(1) Deuteration: Substituting the hydrogen in alkyl chain or phenyl ring with deuterium doubles the effective mass. As a result, the molecular vibration frequency shifts towards a longer wavelength by a factor of $\sqrt{2}$. As reported in Ref. [15], deuteration shifts the CH vibration in alkyl chain ($\sim 3.5 \mu\text{m}$) to $\sim 4.8 \mu\text{m}$, which is unfortunately still in the MWIR region. Therefore, a heavier atom is needed. Nevertheless, deuteration in the

phenyl rings is helpful to shift the absorption in the LWIR to a longer IR region.

- (2) Fluorination: The vibration frequencies of CF, CF₂ and CF₃ occur in the 7–9 μm region. Therefore, fluorination seems to be a promising approach for MWIR LCs. Fluorinated LCs have been commonly used in active matrix LC displays.[25–28] In these compounds, the fluoro substitutions are normally in the (2, 3) positions [for negative $\Delta\epsilon$] or (3,4,5) positions [for positive $\Delta\epsilon$] of a phenyl ring in order to create a large $|\Delta\epsilon|$, while keeping the alkyl chain untouched. As a result, the strong CH vibration absorption bands still exist, although they are not important for display applications. Very little research has been done to tailor fluorinated LCs for MWIR because the molecular design strategies for these two applications (visible wavelength displays and IR phase modulators) are quite different. In 2011, Chen et al. [21] reported a terphenyl compound whose alkyl chains are completely fluorinated. The first compound shows an enantiotropy nematic phase, although its nematic phase is only 2°C. Unfortunately, the overtones of CF, CF₂ and CF₃ appear in the MWIR region. Although the overtone intensity is reduced significantly, it is still noticeable especially when the optical path length is long, such as in a waveguide structure.
- (3) Chlorination: The C–Cl vibration frequency occurs in the 800–600 cm^{-1} range. Thus, its second harmonic is still longer than 6 μm , which is outside the MWIR range. Therefore, from absorption viewpoint C–Cl seems to be a better polar group than CN and CF. Some chlorinated LCs have been developed in the past [24] but these compounds are not suitable for MWIR applications. In this paper, we report some new chlorinated LC compounds and a binary mixture, and measure their absorption loss and physical properties.

2. Molecular design strategies

Here, we use 5CB (4-cyano-4'-pentylbiphenyl) as benchmark for comparison. Figure 1 depicts the measured absorption coefficient of 5CB from 4000 cm^{-1} (2.5 μm) to 650 cm^{-1} (15.38 μm). The measurement was conducted in an isotropic phase in order to avoid scattering and two cells with 100 and 50 μm gaps were employed.

From Figure 1, the carbon-hydrate stretching band (including CH₂ and CH₃) is quite broad (3300–2800 cm^{-1}) and strong, and the peak absorption coefficient exceeds 1000 cm^{-1} . In the centre of MWIR (2500–2000 cm^{-1} , marked as Zone B), the

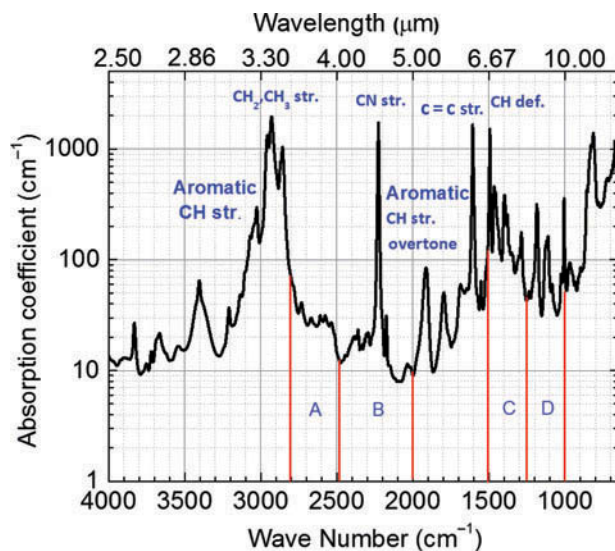


Figure 1. (colour online) Measured absorption coefficient spectrum of 5CB.

$C\equiv N$ stretching shows a narrow but very strong absorption. Cyano is a strong polar group and electron acceptor; it not only provides a large dielectric anisotropy but also helps to boost birefringence. For practical applications, a large $\Delta\epsilon$ helps to reduce operation voltage while high Δn enables a thinner LC layer to be used for reaching the required phase change. Unfortunately, CN has a strong absorption band at $\lambda = 4.45 \mu\text{m}$, so it should be avoided because it raises the baseline absorption. A molecular vibration band usually has Lorentzian shape and its tail could spread broadly. The overlapping of neighbouring bands is responsible for the fairly large baseline absorption.

Besides $C\equiv N$, the baseline absorption in Zone B also comes from the overtone (doubled frequency of a given band or sum frequency of two separated bands) of the absorption bands in Zone D, as marked in Figure 1. As listed in Table 1, the C–C (in the alkyl chain) skeletal stretching ($1300\text{--}700 \text{ cm}^{-1}$) and the in-plane deformation of C–H in the phenyl rings ($1225\text{--}950 \text{ cm}^{-1}$) contribute to the absorption in Zone D. The absorption of Zone C consists of the C–H (in alkyl chain) deformation and C–C skeletal stretching, whose overtone further increases the baseline absorption observed in Zone A. The tail of the absorption band in Zone A may also raise the absorption level in Zone B. Therefore, the absorption in Zones A and B are primarily influenced by four mechanisms: (1) strong CN stretching, (2) absorption tail from the CH stretching of the alkyl chain, (3) absorption tail from the overtone CH stretching of the phenyl ring and (4) the overtone absorption from Zones C and D.

Table 1. Corresponding absorption mechanisms for Zones A–D shown in Figure 1.

Zone	Absorption mechanism	Frequency (cm^{-1})	Wavelength (μm)
A	C–H (in CH_2 , CH_3) def.overtone C–C skeletal str.overtone	2790–2500	3.6–4.0
B	$C\equiv N$ str. C–H (in phenyl ring) in-plane def.overtone C–C (in alkyl chain) skeletal str.overtone	2500–2000	4.0–5.0
C	C–H (in CH_2 , CH_3) def. C–C skeletal str.	1485–1250	6.7–8.0
D	C–H (in phenyl ring) in-plane def. C–C (in alkyl chain) skeletal str.	1250–1000	8.0–10.0

Based on above analyses, we outline the following molecular design strategies to suppress the absorption in Zone B ($2500\text{--}2000 \text{ cm}^{-1}$). Some basic structure elements cannot be removed as they are required to maintain mesogenic phase. The key is to reduce the transition intensity and overlap from these fundamental frequencies and their overtones. The latter is critically important but is often unpredictable beforehand.

2.1 Polar group

We should avoid using $C\equiv N$ or NCS, instead we propose to employ C–F or C–Cl as polar group. The C–F bond shows absorption in the $1400\text{--}1100 \text{ cm}^{-1}$ range. Its overtone may occur at $2200\text{--}2000 \text{ cm}^{-1}$, but it is fairly weak. On the other hand, the absorption band for C–Cl bond is in the range of $800\text{--}600 \text{ cm}^{-1}$, and the second-harmonic overtone will not show up in the $2500\text{--}2000 \text{ cm}^{-1}$ range. Although C–Cl polar group is preferred in terms of absorption, its mesogenic phase is difficult to predict. We need to synthesise several chlorinated structures and examine their LC properties.

2.2 Short alkyl chain

To form LC phase, a flexible side chain and certain length-to-width ratio are required. A too rigid compound usually does not exhibit a mesogenic phase. Even if it does, its melting point could be too high to be practically useful. However, the longer the alkyl chain, the stronger the absorption loss in the MWIR and LWIR regions. Therefore, to suppress the overtone absorption of C–C skeletal stretching, a shorter flexible alkyl chain, e.g., C_2H_5 or C_3H_7 , is preferred. Moreover, with shorter alkyl chain the C–H absorption in both stretching and deformation bands will also be reduced and the tail of CH absorption band is also

suppressed. Thus, a delicate balance between absorption and mesogenic phase needs to be considered.

2.3 Core structure

CH bonds are found in both alkyl chains and aromatic rings. Although a cyclohexane ring helps to widen the nematic range, it contains too many CH bonds and should be avoided from the core structure. To maintain high birefringence, we consider terphenyl as core structure. Moreover, the in-plane deformation of C–H ($1225\text{--}950\text{ cm}^{-1}$) in the phenyl rings occurs when there are two or more adjacent CH bonds. Proper substitutions with F or Cl could avoid the coupling of two or more adjacent CH bonds and reduce the in-plane deformation absorption.

3. LC compounds and mixtures for MWIR

Based on our design strategies, we prepared five fluorinated and two chlorinated terphenyl compounds as listed in Table 2. Also included are their phase transition temperature (PTT) and heat fusion enthalpy (ΔH). To suppress absorption, we replace all the CH bonds in the alkyl chain by $-\text{OCF}_3$, but keep the CH bonds in the phenyl rings in order to obtain nematic phase. Moreover, the CH bonds in the phenyl rings exhibit a much weaker and narrower absorption than those in the flexible alkyl chain.[21] The PTTs were measured by Differential Scanning Calorimetry (TA instruments Q100). The first three compounds have nematic phase. To widen the nematic range, we formulated a eutectic mixture,

Table 2. Chemical structures and properties of the seven compounds studied, where Cr stands for crystalline, N for nematic and I for isotropic phase.

No.	Structure	PTT ($^{\circ}\text{C}$)	ΔH (cal/mol)
1		Cr 86 N 88 I	4921
2		Cr 86 N (84) I ^a	5739
3		Cr 55 N (40) I	4820
4		Cr 113 I	4800
5		Cr 66 I	6583
6		Cr 71 (N 65) I	6421
7		Cr 95 (N 68) I	5848

Note: ^a(0) indicates a monotropic phase.

designated as Mix I, using these five fluoro compounds. The melting point (T_m) is 42°C and clearing point (T_c) is 51.5°C during the heating process. The T_c drops to below -10°C due to supercooling.

To measure MWIR absorption, we filled Mix I to a LC cell with two bare barium fluoride (BaF_2) substrates and measured their transmittance using a Perkin Elmer Spectrum One FTIR Spectrometer. BaF_2 is highly transparent from UV to $\sim 10\text{ }\mu\text{m}$. Its refractive index 1.47 is close to that of LC. The cell gap is $\sim 46\text{ }\mu\text{m}$. To eliminate scattering, we conducted the absorption measurement at an isotropic phase ($\sim 60^{\circ}\text{C}$). To take surface reflections into consideration, we use a single BaF_2 as the reference. Figure 2 shows the measured absorption coefficient of Mix I. Also included in Figure 2 for comparison is 5CB. For Mix I, it shows a relatively low absorption coefficient ($\alpha \sim 2.3\text{ cm}^{-1}$) in the vicinities of 3333 cm^{-1} , i.e., $\lambda \sim 3\text{ }\mu\text{m}$, and the absorption coefficient is smaller than 3 cm^{-1} in the region of $3571\text{--}3333\text{ cm}^{-1}$ ($2.8 \sim 3.0\text{ }\mu\text{m}$). Besides, the absorption at $3030\text{--}2778\text{ cm}^{-1}$ ($3.3 \sim 3.6\text{ }\mu\text{m}$) is significantly reduced because the alkyl chain has been replaced. The absorption peak at 3049 cm^{-1} ($3.28\text{ }\mu\text{m}$) originates from the CH vibration in the phenyl rings. It overlaps with the peak of 5CB very well. Even though the absorption peak resulting from C–O and C–F stretching vibrations are shifted to the $1302\text{--}1156\text{ cm}^{-1}$ ($7.68 \sim 8.65\text{ }\mu\text{m}$),[16] their combination overtone results in a modest ($\sim 80\text{ cm}^{-1}$) but broad absorption peak in the vicinities of $\lambda = 4\text{ }\mu\text{m}$.

To shift overtone resonance peak out of MWIR, we replaced the fluorine with a heavier atom,

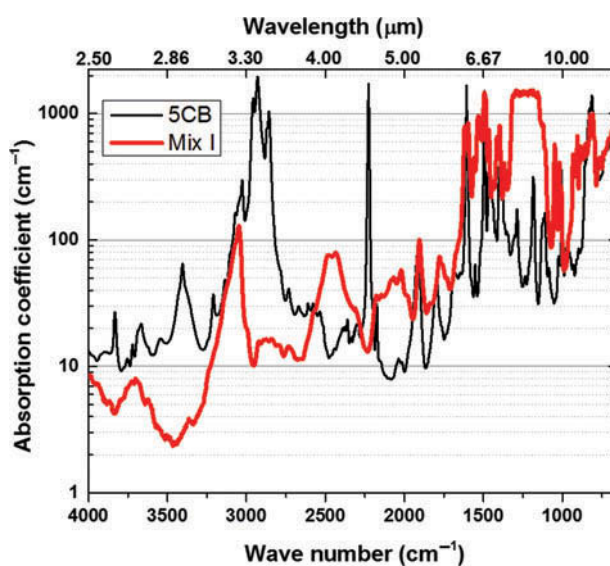


Figure 2. (colour online) Measured absorption coefficient spectrum of 5CB and Mix I.

chlorine. While, for chlorinated compounds, the alkyl chains need to be kept to maintain the flexibility and aspect ratio of the LC compounds. Otherwise, some undesirable properties such as high melting point, large heat fusion enthalpy and high viscosity could occur. More seriously, the compounds may not have any mesogenic phase. The physical properties of chlorinated LC for display applications have been reviewed elsewhere.[24] Thus, we synthesised two chlorinated compounds (#6 and #7) listed in Table 2. Both compounds exhibit monotropic phase. We prepared a binary mixture with 60 wt% compound 6 and 40 wt% compound 7, designated as Mix II. The nematic range of Mix II is from 48.3°C to 69.2°C in the heating process. Supercooling effect lowers the melting point to ~0°C. Thus, Mix II remains LC phase at room temperature (~25°C). To measure the MWIR absorption spectrum, we filled Mix II to a BaF₂ cell with cell gap ~46 μm. The measurement procedures are the same as Mix I.

Figure 3 depicts the measured absorption spectrum of Mix II in the IR region. The absorption spectrum of 5CB is also included for comparison. Mix II exhibits a relative clean absorption in the 4000–3125 cm⁻¹ (2.5 ~ 3.2 μm). The lowest α is 4 cm⁻¹ at 3247 cm⁻¹ (3.08 μm), which is slightly higher than that of Mix I. The responsible absorption mechanism in this region is the CH in-plane deformation. In Mix I, more CH bonds are substituted by C–F bonds so that the in-plane vibration effect is suppressed.

More importantly, Mix II shows a relatively small absorption in 2778–1923 cm⁻¹ (or 3.6 to 5.2 μm) window. The reasons are twofold: (1) In comparison

with 5CB, the CN vibration band centred at 4.45 μm is removed, and (2) In comparison with Mix I, the vibration peaks resulting from C–Cl bonds are shifted to beyond 12.5 μm, and thus the overtone is still outside the MWIR region. The strong resonance peak centred at 2941 cm⁻¹ (3.4 μm) is due to the CH bonds at alkyl chain. Thus, it has similar shape to the resonance peak of 5CB but with weaker amplitude, because 5CB has a longer alkyl chain than the chlorinated compound (#7). Thus, Mix II shows a lower absorption than 5CB in the 4–5-μm MWIR region.

4. Physical properties

In addition to low absorption, the mixture is also required to have high birefringence, low viscosity and modest dielectric anisotropy. Therefore, we also characterised its physical properties.

Birefringence can be obtained by measuring the voltage dependent transmittance (VT) of a homogeneous cell sandwiched between two crossed polarisers. We prepared two homogeneous cells with strong anchoring energy and cell gap $d \sim 5 \mu\text{m}$. In the visible and near IR regions, we can still use indium-tin-oxide-coated glass substrates. Mix I and Mix II were filled into the LC cells at ~70°C and 80°C, respectively. Then, both cells were mounted on a Linkam LTS 350 Large Area Heating/Freezing Stage controlled by TMS94 Temperature Programmer. To obtain maximum transmittance, the LC director was oriented at 45° with respect to the polariser transmission axis. A linearly polarised He–Ne laser ($\lambda = 633 \text{ nm}$), a tunable Argon-ion laser ($\lambda = 514, 488 \text{ and } 457 \text{ nm}$) and a semiconductor laser ($\lambda = 1550 \text{ nm}$) were used as light sources. A 1 kHz square-wave AC signal was applied to the LC cells. The transmitted light was measured by a photodiode detector and recorded by a LabVIEW data acquisition system (DAQ, PCI6110). Thus, the corresponding VT curves and phase retardation were measured. The birefringence at a given wavelength and temperature was obtained from the phase retardation based on Equation (1).[29]

The temperature dependent birefringence for Mix II was measured from 25°C to 65°C, and the results for $\lambda = 633 \text{ nm}$ are plotted in Figure 4, where dots are experimental data and solid line is the fitting curve based on Haller's semi-empirical equation [30]:

$$\Delta n = \Delta n_0(1 - T/T_c)^\beta \quad (4)$$

where Δn_0 is the extrapolated birefringence at $T = 0 \text{ K}$ and β is a material constant. Through fitting, we find $\Delta n_0 = 0.303$ and $\beta = 0.153$.

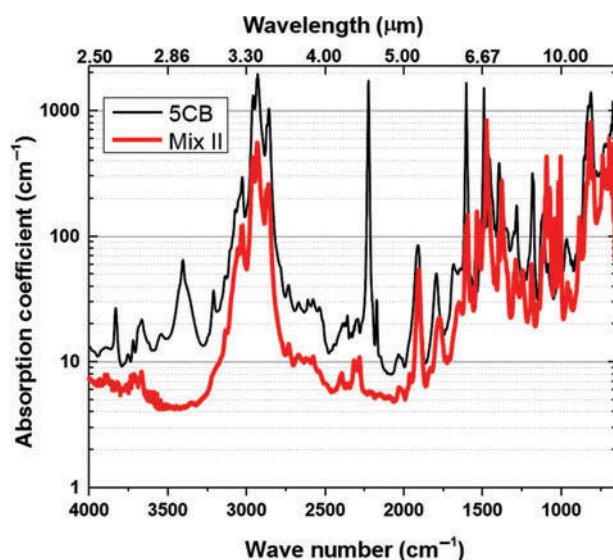


Figure 3. (colour online) Measured absorption coefficient of 5CB and Mix II.

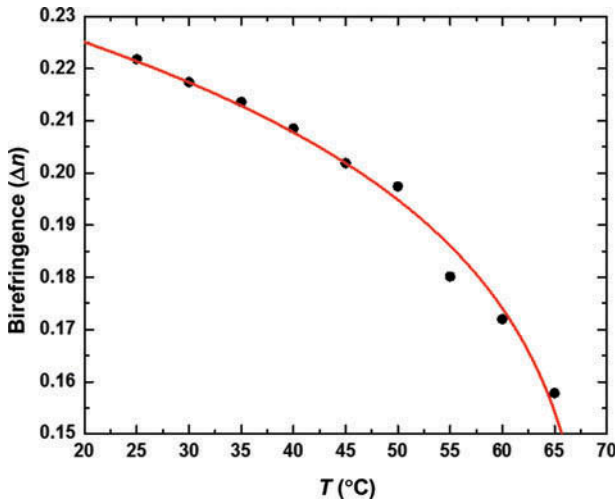


Figure 4. (colour online) Temperature dependent birefringence of Mix II at $\lambda = 633$ nm: dots stand for measured data and solid line for fitting curve with Equation (4).

To determine the birefringence in the MWIR region, we measured the dispersion curve using several visible and short-wave IR lasers at 25°C. Results are plotted in Figure 5. Dots are measured data at five discrete wavelengths and solid curve represents the fitting results using the following single-band model [12]:

$$\Delta n = G \frac{\lambda^2 \lambda^{*2}}{\lambda^2 - \lambda^{*2}} \tag{5}$$

where G is a proportionality constant and λ^* is the mean resonance wavelength. Through fitting, we find $G = 3.05 \mu\text{m}^{-2}$ and $\lambda^* = 0.249 \mu\text{m}$. Based on these

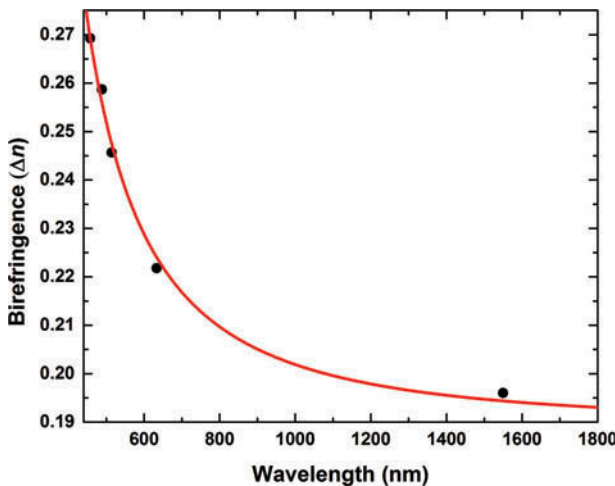


Figure 5. (colour online) Birefringence dispersion of Mix II at room temperature: dots are measured data and solid line is fitting with Equation (5).

parameters, the birefringence at any wavelength can be calculated through Equation (5). In the MWIR region in which $\lambda \gg \lambda^*$, the birefringence is decreased to a plateau,[13] its value is about 10–20% lower than that in the visible region. For Mix II, the birefringence in the MWIR region is still relatively high ($\Delta n \sim 0.19$). Higher birefringence enables a thinner cell gap to be used for achieving a certain phase change, say 2π , which in turn helps improve response time. We also measured the birefringence of Mix I, and its $\Delta n = 0.17$ at $T = 25^\circ\text{C}$ and $\lambda = 633$ nm, which is much smaller than that of Mix II ($\Delta n = 0.22$).

The visco-elastic coefficient (γ_1/K_{11}) was obtained by measuring the dynamic free relaxation time for a controlled phase change as [31]:

$$\delta(t) = \delta_0 \exp\left(-\frac{2t}{\tau_0}\right) \tag{6}$$

$$\tau_0 = \frac{\gamma_1 d^2}{K_{11} \pi} \tag{7}$$

where δ_0 is the total phase change, t_0 is the relaxation time, γ_1 is rotational viscosity and K_{11} is the splay elastic constant. We plot visco-elastic coefficient for Mix II at different temperatures in Figure 6, where dots are experimental data and solid line is fitting curve with following equation:

$$\frac{\gamma_1}{K_{11}} = A \frac{\exp(E/K_B T)}{(1 - T/T_C)^\beta} \tag{8}$$

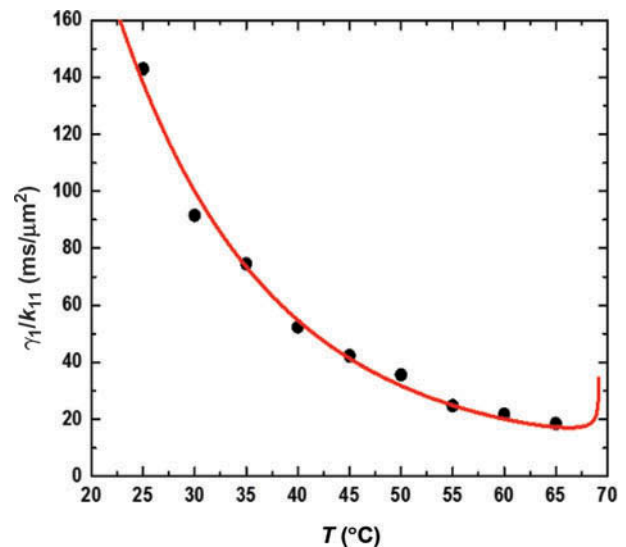


Figure 6. (colour online) Temperature dependent visco-elastic coefficient of Mix II: dots are measured data and solid line is fitting with Equation (8). $\lambda = 633$ nm.

In Equation (8), A is a proportional constant, E is the activation energy, T is the Kelvin temperature and K_B is the Boltzmann constant. For Mix II, we find $A = 1.11 \times 10^{-7} \text{ ms}/\mu\text{m}^2$ and $E = 531 \text{ meV}$. Mix II has a much larger visco-elastic coefficient ($\sim 140 \text{ ms}/\mu\text{m}^2$) than Mix I ($\sim 25 \text{ ms}/\mu\text{m}^2$) at room temperature. The possible explanations are: (1) the chlorine atom is heavier and bulkier than fluorine and (2) the chloro compounds have longer alkyl chain. As the temperature increases, the visco-elastic coefficient decreases significantly.

To determine the dielectric anisotropy, we measured the capacitance of a homogenous cell and a homeotropic cell using an HP-4274 multi-frequency LCR meter. For Mix II, $\Delta\epsilon = 7.82$ at 25°C . This medium dielectric anisotropy results from the modest C–Cl dipole group. Mix I aligns well in homogeneous cells, but not so well in homeotropic cells. Therefore, we can only estimate its $\Delta\epsilon$ value through the measured threshold voltage ($3.4 V_{\text{rms}}$) from a homogeneous cell. The estimated $\Delta\epsilon$ is about 4. This small $\Delta\epsilon$ value can be easily understood because some compounds listed in Table 2 have dipoles on both terminal groups. As a result, their dipole moments cancel each other.

5. Conclusion

We have prepared two LC mixtures for MWIR applications. For the fluorinated mixture Mix I, it shows a relatively small absorption coefficient (2.5 cm^{-1}) window at $\lambda \sim 3 \mu\text{m}$. However, the overtone absorption of CF band occurs in the vicinities of $4 \mu\text{m}$. Therefore, Mix I is more suitable for $\lambda \sim 3 \mu\text{m}$ operation. For the chlorinated LC mixtures, Mix II shows a low absorption window ($\alpha < 5 \text{ cm}^{-1}$) in the $4\text{--}5 \mu\text{m}$ region. Besides, it also possesses other attractive physical properties, such as high birefringence, modest positive dielectric anisotropy and broad nematic temperature range. Therefore, these new LC mixtures are attractive candidates for MWIR applications, but at different windows.

Funding

This work was supported by Office of Naval Research (ONR) [contract number N00014-13-1-0096].

References

[1] Efron U. Spatial light modulator technology: materials, devices, and applications. Boca Raton (FL): CRC Press; 1994.

- [2] Mcmanamon PF, Dorschner TA, Corkum DL, Friedman LJ, Hobbs DS, Holz M, Liberman S, Nguyen HQ, Resler DP, Sharp RC, Watson EA. Optical phased array technology. *Proc IEEE*. 1996;84:268–298. doi:10.1109/5.482231
- [3] Resler D, Hobbs D, Sharp R, Friedman L, Dorschner T. High-efficiency liquid-crystal optical phased-array beam steering. *Opt Lett*. 1996;21:689–691. doi:10.1364/OL.21.000689
- [4] Ren H, Wu S-T. Introduction to adaptive lenses. Hoboken (NJ): Wiley; 2012.
- [5] Dolfi D, Labeyrie M, Joffre P, Huignard JP. Liquid crystal microwave phase shifter. *Electron Lett*. 1993;29:926–928. doi:10.1049/el:19930618
- [6] Lim KC, Margerum JD, Lackner AM. Liquid crystal millimeter wave electronic phase shifter. *Appl Phys Lett*. 1993;62:1065–1067. doi:10.1063/1.108796
- [7] Chen C-Y, Hsieh C-F, Lin Y-F, Pan R-P, Pan C-L. Magnetically tunable room-temperature 2 pi liquid crystal terahertz phase shifter. *Opt Express*. 2004;12:2625–2630. doi:10.1364/OPEX.12.002625
- [8] Lin X, Wu J, Hu W, Zheng Z, Wu Z, Zhu G, Xu F, Jin B, Lu Y. Self-polarizing terahertz liquid crystal phase shifter. *AIP Adv*. 2011;1:032133. doi:10.1063/1.3626560
- [9] Dąbrowski R, Kula P, Herman J. High birefringence liquid crystals. *Crystals*. 2013;3:443–482. doi:10.3390/cryst3030443
- [10] Chao T-H, Lu TT, Davis SR, Rommel SD, Farca G, Luey B, Martin A, Anderson MH, Casasent DP, Chao T. Compact liquid crystal waveguide based fourier transform spectrometer for in-situ and remote gas and chemical sensing. *Proc SPIE*. 2008;6977:69770P. doi:10.1117/12.785888
- [11] Davis SR, Farca G, Rommel SD, Johnson S, Anderson MH. Liquid crystal waveguides: new devices enabled by >1000 waves of optical phase control. *Proc SPIE*. 2010;7618:E1–E14.
- [12] Wu S-T. Birefringence dispersions of liquid crystals. *Phys Rev A*. 1986;33:1270–1274. doi:10.1103/PhysRevA.33.1270
- [13] Li J, Wu S-T, Brugioni S, Meucci R, Faetti S. Infrared refractive indices of liquid crystals. *J Appl Phys*. 2005;97:073501
- [14] Wu S-T. Absorption measurements of liquid crystals in the ultraviolet, visible, and infrared. *J Appl Phys*. 1998;84:4462–4465. doi:10.1063/1.368671
- [15] Wu S-T. Infrared properties of nematic liquid crystals: an overview. *Opt Eng*. 1987;26:120–128. doi:10.1117/12.7974037
- [16] Mistry B. Handbook of spectroscopic data chemistry: UV, IR, PMR, CNMR and mass spectroscopy. Jaipur: Oxford; 2009.
- [17] Jakeman E, Raynes E. Electro-optic response times in liquid crystals. *Phys Lett A*. 1972;39:69–70. doi:10.1016/0375-9601(72)90332-5
- [18] Wu S-T, Wang Q-H, Kempe MD, Kornfield JA. Perdeuterated cyanobiphenyl liquid crystals for infrared applications. *J Appl Phys*. 2002;92:7146–7148. doi:10.1063/1.1521512
- [19] Gray GW, Mosley A. The synthesis of deuterated 4-n-alkyl-4'-cyanobiphenyls. *Mol Cryst Liq Cryst*. 1978;48:233–242. doi:10.1080/00268947808083764
- [20] Thomas AF. Deuterium labeling in organic chemistry. New York (NY): Appleton-Century-Crofts; 1971.
- [21] Chen Y, Xianyu H, Sun J, Kula P, Dabrowski R, Tripathi S, Twieg RJ, Wu S-T. Low absorption liquid

- crystals for mid-wave infrared applications. *Opt Express*. 2011;19:10843–10848. doi:[10.1364/OE.19.010843](https://doi.org/10.1364/OE.19.010843)
- [22] Hird M. Fluorinated liquid crystals—properties and applications. *Chem Soc Rev*. 2007;36:2070–2095. doi:[10.1039/b610738a](https://doi.org/10.1039/b610738a)
- [23] Coates D, Greenfield S, Sage I, Smith G, Doane JW, Yaniv Z. Liquid crystal mixtures for polymer matrix displays. *Liq Cryst Disp Appl*. 1990;1257:37–45. doi:[10.1117/12.19925](https://doi.org/10.1117/12.19925)
- [24] Wu S-T, Coates D, Bartmann E. Physical properties of chlorinated liquid crystals. *Liq Cryst*. 1991;10:635–646. doi:[10.1080/02678299108241731](https://doi.org/10.1080/02678299108241731)
- [25] Chen Y, Sun J, Xianyu H, Wu S-T, Liang X, High Birefringence TH. Fluoro-terphenyls for thin-cell-gap TFT-LCDs. *J Display Technol*. 2011;7:478–481. doi:[10.1109/JDT.2011.2150197](https://doi.org/10.1109/JDT.2011.2150197)
- [26] Chen Y, Peng F, Wu S-T. Submillisecond-response vertical-aligned liquid crystal for color sequential projection displays. *J Display Technol*. 2013;9:78–81. doi:[10.1109/JDT.2013.2243403](https://doi.org/10.1109/JDT.2013.2243403)
- [27] Chen Y, Luo Z, Peng F, Wu S-T. Fringe-field switching with a negative dielectric anisotropy liquid crystal. *J Display Technol*. 2013;9:74–77. doi:[10.1109/JDT.2013.2242844](https://doi.org/10.1109/JDT.2013.2242844)
- [28] Schadt M. Liquid crystal materials and liquid crystal displays. *Annu Rev Mater Sci*. 1997;27:305–379. doi:[10.1146/annurev.matsci.27.1.305](https://doi.org/10.1146/annurev.matsci.27.1.305)
- [29] Wu S-T, Efron U, Hess LD. Birefringence measurements of liquid crystals. *Appl Opt*. 1984;23:3911–3915. doi:[10.1364/AO.23.003911](https://doi.org/10.1364/AO.23.003911)
- [30] Haller I. Thermodynamic and static properties of liquid crystals. *Prog Solid State Chem*. 1975;10:103–118. doi:[10.1016/0079-6786\(75\)90008-4](https://doi.org/10.1016/0079-6786(75)90008-4)
- [31] Wu S-T, Wu C-S. Experimental confirmation of the Osipov–Terentjev theory on the viscosity of nematic liquid crystals. *Phys Rev A*. 1990;42:2219–2227. doi:[10.1103/PhysRevA.42.2219](https://doi.org/10.1103/PhysRevA.42.2219)